Smartphone-based infrared thermography: technical validation and canine cadaver proof of concept

Smartphone-gekoppelde infraroodthermografie: technische validatie en hondenkadaver proof-of-concept

[1,2]T.B. Dadi, [1]A. Engels, [1]H. de Rooster

[1]Small Animal Department, Faculty of Veterinary Medicine, Ghent University, Salisburylaan 133, Merelbeke B-9820, Belgium

[2]Veterinary Clinical Division, Faculty of Veterinary Medicine, Universitas Airlangga, Kampus C Mulyorejo, Surabaya 60115, Indonesia

bhawono@fkh.unair.ac.id/ tribhawono.dadi@ugent.be

ABSTRACT

Infrared thermography (IRT) may provide an objective tool for detecting surface temperature patterns during surgical assessment, but data on low-cost smartphone-attached systems in veterinary medicine are scarce. In this experimental ex vivo study, a smartphone-attached infrared camera (InfiRay P2 Pro) was evaluated against a contact thermometer in controlled water baths and in a canine jejunal cadaver model. In two water-bath setups (2.9 L at 20 cm; 1.5 L at 30 cm), the average and point temperature outputs showed very high correlation and agreement with the reference thermometer (bias <1.0 °C, intraclass correlation coefficient ≥0.98), whereas minimum temperature underestimated and maximum temperature slightly overestimated bulk water temperature. In the cadaver model, the camera detected clear localized increases in jejunal surface temperature after intraluminal and mesenteric venous warming. These preliminary results indicate that low-cost smartphone-attached IRT can detect local thermal contrast, although further in vivo validation is required before clinical use for intestinal viability assessment.

SAMENVATTING

Infraroodthermografie (IRT) kan een objectief hulpmiddel zijn voor het detecteren van oppervlaktetemperatuurpatronen tijdens chirurgische beoordeling, maar gegevens over goedkope smartphone-gekoppelde systemen zijn schaars in de diergeneeskunde. In deze experimentele ex-vivostudie werd een smartphone-gekoppelde infraroodcamera (InfiRay P2 Pro) vergeleken met een contactthermometer in gecontroleerde omstandigheden in een waterbad en in een hondenkadavermodel. In twee waterbadopstellingen (2,9 L op 20 cm; 1,5 L op 30 cm) vertoonden de gemiddelde en punttemperatuurwaarden een zeer hoge correlatie en goede overeenkomst met de referentiethermometer (i. e. bias <1,0 °C, nauwe overeenstemmingsgrenzen, intra-class correlatiecoëfficiënt ≥0,98), terwijl de minimumtemperatuur de gemiddelde watertemperatuur onderschatte en de maximumtemperatuur deze licht overschatte. In het kadavermodel detecteerde de camera duidelijke, gelokaliseerde stijgingen van de jejunale oppervlaktetemperatuur na intraluminale of intraveneuze opwarming. Deze eerste resultaten geven aan dat goedkope smartphone-gekoppelde IRT lokale thermische contrasten kan detecteren, hoewel verdere in-vivovalidatie moet worden uitgevoerd voordat het klinisch gebruik voor de intestinale levensvatbaarheid kan worden onderzocht.

INTRODUCTION

Infrared thermography (IRT) is a non-contact imaging modality used in medicine to detect long-wave infrared radiation emitted from the body surface and converting it into a temperature map. In healthy individuals, skin temperature is maintained within a relatively narrow range by autonomic regulation of vasodilatation and vasoconstriction (Bagavathiappan et al., 2009; Fernández-Cuevas et al., 2015). By visualizing superficial temperature gradients with high spatial resolution, IRT may reveal surface temperature patterns associated with regional changes in blood flow and tissue perfusion, without ionizing radiation or the need for contrast agents (Bagavathiappan et al., 2009; Fernández-Cuevas et al., 2015). In human medicine, IRT has been used as an adjunctive tool in the diagnosis of breast cancer, diabetic neuropathy and peripheral vascular disorders (Lahiri et al., 2012). In wound care and soft-tissue assessment, thermography has been investigated as a non-contact method to quantify local temperature patterns associated with inflammation, infection, perfusion changes and tissue compromise, particularly in surgical wounds, diabetic foot ulcers, pressure injuries and burns (Ramirez-GarciaLuna et al., 2022; Fridberg et al., 2024; Rahman et al., 2025). In these and other conditions, changes in microcirculation and autonomic vasomotor activity can lead to altered heat patterns, which may be detected as localized areas of hyper- or hypothermia (Bagavathiappan et al., 2009; Fernández-Cuevas et al., 2015).

In veterinary medicine, IRT has attracted increasing interest as a non-invasive adjunct for the assessment of locomotor disorders, pain and inflammation, wound healing and peripheral vascular integrity in companion, production and laboratory animals (Loughin and Marino, 2007; Rekant et al., 2016; McManus et al., 2016; Casas-Alvarado et al., 2020; Mota-Rojas et al., 2021). Case reports, experimental and clinical studies have shown that IRT can visualize temperature changes associated with lameness, bone neoplasia, digital dermatitis and other inflammatory processes, and may contribute to lesion localization or to objective monitoring of treatment response (Redaelli et al., 2014; McManus et al., 2016; Giggin et al., 2023). More recently, thermography has also been investigated as a means of monitoring surgical wounds and flaps and of evaluating regional vascular compromise and peri-operative pain in companion animal patients (Casas-Alvarado et al., 2020).

A clinical scenario in small animal surgery where IRT could be particularly valuable is the intra-operative assessment of intestinal viability. Dogs frequently present with small intestinal obstruction due to foreign bodies or other causes, and surgical decision-making hinges on whether a given segment is salvageable or requires resection (Finstad et al., 2023). At present, surgeons primarily rely on subjective criteria such as serosal color, mural thickness, peristalsis, and bleeding from enterotomies or marginal vessels, all of which are prone to inter-observer variability and can be misleading when perfusion is borderline (Casas-Alvarado et al., 2020; Mullen et al., 2020). Human surgical literature indicates that more accurate delineation of the border between viable and non-viable bowel reduces the incidence of anastomotic failure and ischemic complications (Urbanavičius et al., 2011). In a porcine model of mesenteric ischemia, IRT has been shown to identify the transition between perfused and non-perfused intestine, supporting its potential for visualizing thermal demarcation between intestinal segments (Bernard et al., 2019).

To date, veterinary IRT research has predominantly relied on dedicated, high-resolution infrared cameras, as illustrated by the equipment described in reviews of musculoskeletal, dermatologic and welfare applications in companion and farm animals (Rekant et al., 2016; McManus et al., 2016; Casas-Alvarado et al., 2020). In parallel, compact infrared sensors that connect directly to smartphones, such as the FLIR One® family, have become commercially available and are marketed as more affordable, portable alternatives to conventional thermographic cameras (Huynh, 2019; Teledyne FLIR, 2024). Within human medicine, smartphone-attached IRT has been used for peripheral vascular and soft-tissue assessment, including thermal screening of ischemic or inflamed regions, whereas in veterinary medicine such devices have been explored in horses to monitor limb surface temperature and to evaluate regional nerve blocks as part of lameness investigations (Huynh, 2019; Ferlini Agne et al., 2024). In dogs, early protocol-based thermographic work used a dedicated infrared camera and standardized ROI assessment to describe reproducible limb temperature patterns (Loughin and Marino, 2007). In horses, comparison of a high-resolution infrared camera with a smartphone infrared device after median nerve anesthesia showed changes in skin surface temperature, but the smartphone device produced higher and more variable temperature outputs; caution was therefore advised for clinical interpretation (Ferlini Agne et al., 2024).

In several experimental and clinical studies, high-end infrared cameras have been used to evaluate intestinal perfusion or other surgical problems in animals and humans (Bagavathiappan et al., 2009; Bernard et al., 2019; Finstad et al., 2023), but these devices remain expensive and are not widely available in general veterinary practice. At the same time, low-cost smartphone-based infrared cameras have become commercially available and are increasingly marketed to veterinarians, yet their technical performance has not been validated against reference thermometry in controlled conditions, and their ability to detect local intestinal temperature differences in dogs has not yet been investigated. To address this gap, the aims of this study were (i) to perform a technical validation of a smartphone-attached infrared camera against a calibrated digital thermometer in a controlled water-bath model, and (ii) to provide a proof of concept that the camera can visualize local surface temperature differences in a canine jejunal cadaver model mimicking intra-operative conditions. By focusing on a low-cost, portable system, this study

seeks to provide a realistic foundation for the future integration of IRT into small animal surgical practice.

MATERIALS AND METHODS

Infrared camera and reference thermometer

All thermal images were obtained using a smartphone-attached infrared camera (InfiRay P2 Pro, InfiRay Technologies Co., Ltd., China). According to the manufacturer's specifications, the device has an infrared resolution of 256 × 192 pixels, a thermal sensitivity of approximately 40 mK, a frame rate of 25 Hz and a stated measurement accuracy of ±2°C. The device converts long-wave infrared radiation into a digital image and provides numerical temperature outputs per pixel. The images were acquired and analyzed using the manufacturer's P2 Pro mobile application, version 1.1.3.240316. For each image, the manufacturer's software allowed definition of a rectangular region of interest (ROI), from which four parameters were extracted: minimum (Min), maximum (Max), average (Avg) and Point (Pt)) temperature. ROI placement was performed manually and kept within the target surface visible on each thermal image. For quantitative water-bath measurements, the ROI was positioned centrally on the water surface, whereas point measurements were placed close to the reference thermometer probe. For cadaver images, point measurements were placed on visually defined regions representing the warmed jejunal segment and adjacent non-manipulated intestine.

A calibrated digital thermometer (Testo 735, Testo SE & Co. KGaA, Germany) equipped with an immersion probe was used as reference standard. Before each experiment, the thermometer was checked according to the manufacturer's recommendations. For all measurements, the emissivity on the infrared camera was set to 0.95, which is commonly used for water and biological soft tissues. All recordings were performed indoors under stable ambient conditions, without direct sunlight or draughts.

Figure 1. Overview of the experimental setup.

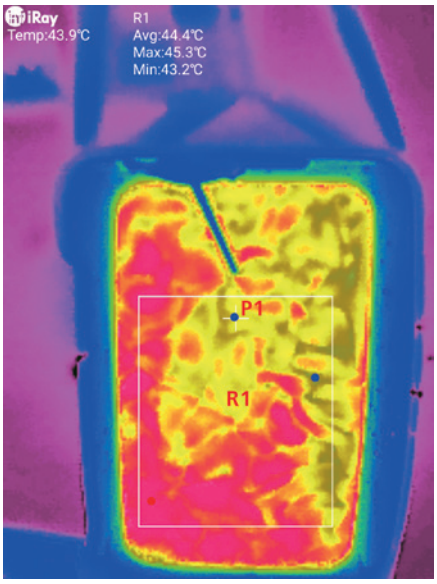

Figure 2. Thermal image acquired with the InfiRay P2 Pro during the first measurement. The white rectangle (R1) indicates the region of interest (ROI) used to extract minimum, maximum and average temperatures; P1 indicates the point measurement location. Colors represent a temperature gradient from cooler to warmer values. The thermometer probe appears cooler than the surrounding water.

Water-bath validation experiment

A controlled water-cooling model was used to evaluate the agreement between the infrared camera and the reference thermometer over a clinically relevant temperature range. Two tests were performed that differed in water volume and camera distance.

In Test 1, 2.9 L of tap water was poured into a plastic container, resulting in a water depth of 7 cm. The infrared camera was positioned 20 cm above the water surface and oriented perpendicular to it. In Test 2, 1.5 L of tap water was used, yielding a water depth of 3.5 cm, with the camera positioned 30 cm above the surface. In both tests, the immersion probe of the Testo 735 was placed centrally in the water column at a depth of about 1 cm below the surface, avoiding contact with the container wall and bottom, and secured to prevent movement (Figure 1).

In each test, the water was heated on a stove to approximately 45 °C while being gently stirred to achieve a

visually homogeneous temperature, which was confirmed by repeated measurements with the Testo 735. The container was then removed from the heat source and placed on an insulated surface. The water was allowed to cool passively from about 45 °C to just below 30 °C. During this cooling phase, paired measurements were obtained at 1-minute intervals. At each time point, the temperature recorded by the Testo 735 was noted, and a thermal image of the water surface was captured. A central rectangular ROI was drawn on the water surface, avoiding the container rim, visible reflections, the thermometer shaft, and edge artefacts. For the average (Avg) output, the ROI excluded the thermometer probe itself (Figure 2). For the point (Pt) output, a single point was placed close to the probe tip. Thus, the Testo 735 measured water temperature approximately 1 cm below the surface, whereas the infrared camera measured the water surface.

For each test, the minimum (Min), maximum (Max), Avg and Pt temperatures reported for this ROI were exported and matched to the corresponding thermometer reading for subsequent statistical analysis. The analysis workflow was therefore: image acquisition, manual ROI or point selection, extraction of Min, Max, Avg and Pt temperature values, matching with the corresponding Testo 735 reading, and agreement analysis.

Cadaver jejunal thermal contrast model

To mimic a clinical setting, an intestinal perfusion model was created using a canine cadaver. Ethical approval was not required because no live animal was used. The dog had been euthanized shortly before the experiment for reasons unrelated to this study; the owner consented to donate the cadaver for scientific use. At the start of the procedure, the internal abdominal temperature and ambient room temperature, measured with the calibrated Testo 735 thermometer, were 37.5 °C and 22.3 °C, respectively. The cadaver was positioned in dorsal recumbency, the ventral abdomen was clipped, and the intended incision site was covered with surgical drapes. The same infrared camera as in the water-bath experiment InfiRay P2 Pro was used throughout this experiment.

A midline abdominal incision of approximately 20 cm was made with a scalpel through skin, subcutis and linea alba, starting at the sternum and extending caudally along the linea alba. A 30 cm segment of jejunum was lifted out of the abdomen. To minimize background heat from the cadaver on the infrared images, a sheet of cardboard was placed underneath the exposed intestinal loop. Two ligatures were then applied around the isolated intestinal loop to create a ligated jejunal segment of approximately 7 cm in length.

A purse-string suture was preplaced in the distal third of this segment, and the probe of the Testo thermometer was introduced through the center of the purse string into the intestinal lumen and then the purse-string suture was tightened to secure the probe. Subsequently, approximately 7 mL of warm water were injected into the compartment using a 21G needle attached to a 20 mL syringe. The temperature of the warmed compartment and of the adjacent, non-warmed intestinal tissue was measured with the InfiRay P2 Pro using Pt measurements. Infrared images were obtained immediately before and after the intraluminal injection.

Next, a mesenteric vein supplying a jejunal segment was cannulated with a 24G catheter, which was secured in place with a ligature. The vein was ligated around the catheter to prevent backflow. Warm water was slowly injected into the vein with a syringe, and the resulting temperature changes were recorded as a video sequence and still images with the InfiRay P2 Pro.

After this procedure, the catheter and associated ligatures were removed, and the jejunum was returned to the abdominal cavity. A new jejunal segment was then exteriorized. Two encircling ligatures were placed with an approximate spacing of 9 cm to isolate the segment, and approximately 10 mL of warm water were injected intraluminally. The intestinal segment was subsequently reintroduced into the abdomen. Backhaus clamps were used to retract the abdominal wall and widen the incision for imaging. Using the infrared camera, the temperature difference between the water-injected intestinal segment and the surrounding, non-manipulated intestines in situ was visually assessed with Pt measurements and the corresponding temperature difference ($\Delta T = P1 - P2$) was reported to illustrate the magnitude of the thermographic contrast. These point measurements were used to describe the magnitude of local thermal contrast and were not intended to define diagnostic thresholds.

Statistical analysis

All statistical analyses were performed in RStudio (version 2025.09.2, “Cucumberbed Sunflower”; Posit Software, PBC). For the water-bath validation experiment, agreement between the infrared camera outputs (minimum (Min), maximum (Max), average (Avg) and point (Pt) and the reference thermometer was evaluated separately for Test 1 (2.9 L at 20 cm) and Test 2 (1.5 L at 30 cm). Agreement was assessed primarily using Bland–Altman analysis, reporting the mean bias (camera − thermometer) and 95% limits of agreement (mean difference ± 1.96 × SD of the differences), and the results were visualized in Bland-Altman plots. Because the water-bath measurements were obtained serially during passive cooling, consecutive observations were not fully independent. Therefore, the agreement statistics were interpreted descriptively within the tested temperature range. Normality of the paired differences (camera − thermometer) was assessed using Q–Q plots and the Shapiro–Wilk test ($\alpha = 0.05$), with Anderson-Darling and Lilliefors tests used as sensitivity checks. When the distribution of paired differences deviated from normality, Bland-Altman plots were used for the visual assessment of agreement, and the limits of agreement were interpreted cautiously as descriptive estimates rather than as strict inferential thresholds. The magnitude

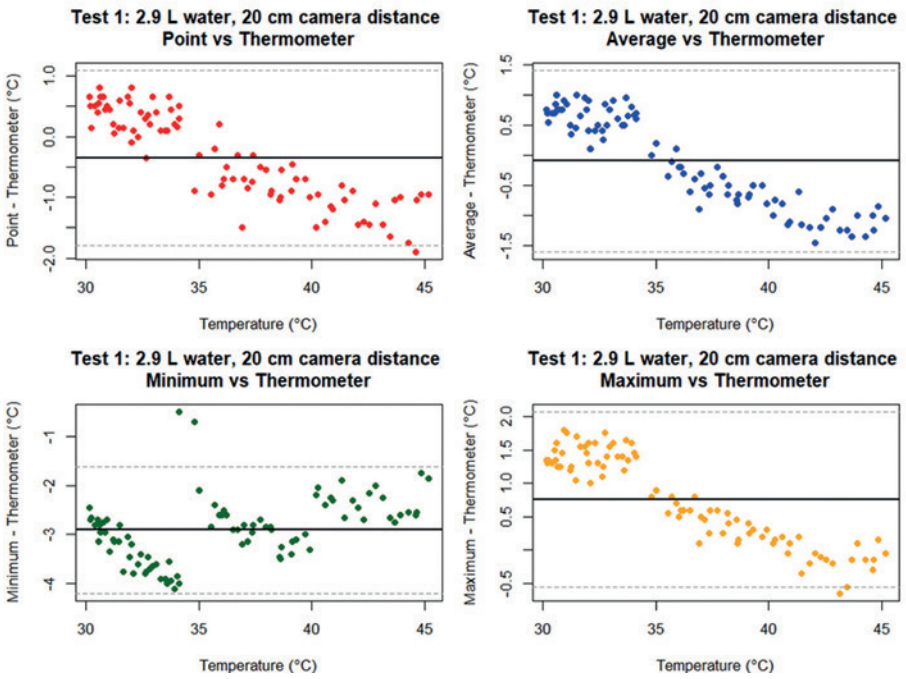

Figure 3. Bland-Altman plots for Test 1 (2.9 L water, 20 cm camera distance) comparing infrared camera outputs with the reference thermometer. Each dot represents one paired measurement, with the thermometer value on the x-axis and the difference (IR-thermometer, °C) on the y-axis. Panels show (top left) point temperature, (top right) average temperature, (bottom left) minimum temperature, and (bottom right) maximum temperature. The solid horizontal line represents the mean bias, and the dashed lines indicate the 95% limits of agreement.

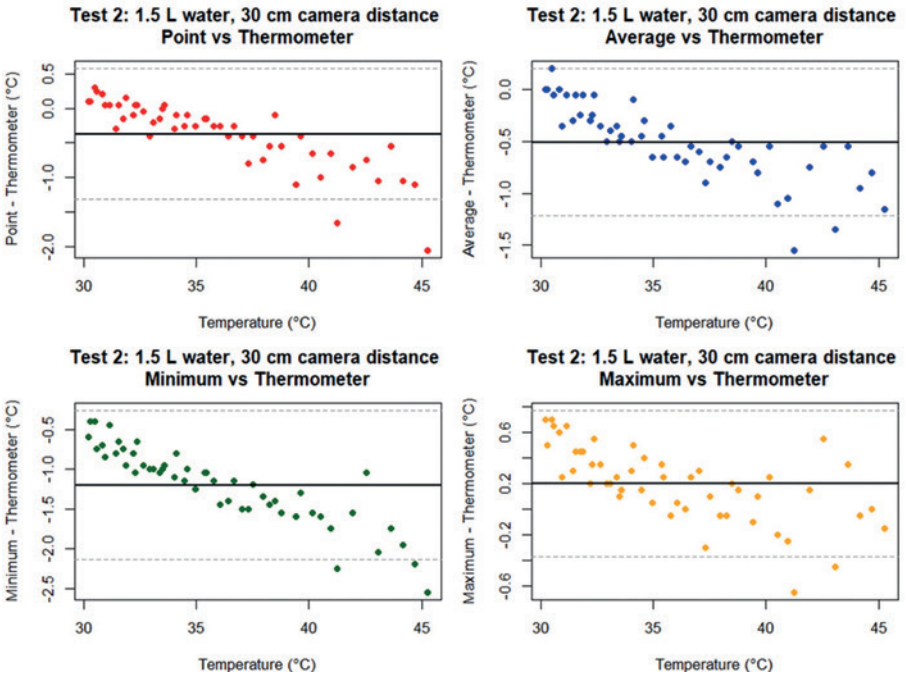

Figure 4. Bland-Altman plots for Test 2 (1.5 L water, 30 cm camera distance) comparing infrared camera outputs with the reference thermometer. Each dot represents one paired measurement, with the thermometer value on the x-axis and the difference (IR-thermometer, °C) on the y-axis. Panels show (top left) point temperature, (top right) average temperature, (bottom left) minimum temperature, and (bottom right) maximum temperature. The solid horizontal line represents the mean bias, and the dashed lines indicate the 95% limits of agreement.

of disagreement was summarized using the root mean square error (RMSE = √mean[(camera − thermometer)^2]). Reliability between the thermometer and each camera output was quantified using intraclass correlation coefficients (ICC; two-way random-effects, absolute-agreement, single-measurement) with 95% confidence intervals. Spearman rank correlation coefficient (ρ) was reported descriptively to characterize association between the camera outputs and the reference thermometer.

RESULTS

Water-bath validation experiment

Across both tests, all infrared camera outputs showed very strong association with the reference thermometer, with Spearman correlation coefficients (ρ) ≥ 0.995 for all comparisons (Table 1). Bland-Altman agreement between the camera outputs and the reference thermometer is illustrated in Figures 3 and 4. In Test 1 (2.9 L at 20 cm), the Avg and Pt outputs demonstrated the best overall agreement with the thermometer. Avg showed a small mean bias of −0.10 °C with 95% limits of agreement (LoA) from −1.60 to 1.41 °C, RMSE 0.77 °C and ICC 0.983 (95% CI 0.974–0.989). Pt similarly showed a bias of −0.35 °C (LoA −1.80 to 1.09 °C), RMSE 0.81 °C and ICC 0.981 (95% CI 0.962–0.990). Max slightly overestimated the thermometer (bias 0.76 °C) while maintaining narrow LoA, low RMSE (1.00 °C) and high reliability (ICC 0.972, 95% CI 0.716–0.991). In contrast, Min consistently underestimated the thermometer, with a large negative bias (−2.90 °C), wide LoA (−4.19 to −1.61 °C), the highest RMSE (2.97 °C), and the least robust ICC estimate (0.829, 95% CI −0.015 to 0.960).

In Test 2 (1.5 L at 30 cm), Max showed the smallest overall error (RMSE 0.35 °C) and excellent reliability (ICC 0.997, 95% CI 0.988–0.999), while Avg and Pt again showed small negative biases (−0.50 °C and −0.36 °C, respectively), relatively narrow LoA and high ICC values (both 0.989). Min still underestimated the thermometer (bias −1.20 °C; LoA −2.14

Table 1. Agreement between infrared camera outputs and the reference thermometer in heated water under two experimental conditions: Test 1 (2.9 L water, 20 cm camera distance) and Test 2 (1.5 L water, 30 cm camera distance). Spearman correlation coefficients, root mean square error (RMSE), mean bias, 95% limits of agreement (LoA) and intraclass correlation coefficients (ICC) are shown for each comparison.

Test 1 (2.9 L water, 20 cm; n = 87)						
Method	**n**	**Spearman ρ**	**RMSE (°C)**	**Bias (°C)**	**95% LoA (°C)**	**ICC (95% CI)**
Thermometer vs Minimum	87	0.995	2.97	−2.90	−4.19 to −1.61	0.829 (−0.015 to 0.960)
Thermometer vs Maximum	87	0.999	1.00	0.76	−0.55 to 2.07	0.972 (0.716 to 0.991)
Thermometer vs Average	87	0.998	0.77	−0.10	−1.60 to 1.41	0.983 (0.974 to 0.989)
Thermometer vs Point	87	0.996	0.81	−0.35	−1.80 to 1.09	0.981 (0.962 to 0.990)
Test 2 (1.5 L water, 30 cm; n = 51)						
Method	**n**	**Spearman ρ**	**RMSE (°C)**	**Bias (°C)**	**95% LoA (°C)**	**ICC (95% CI)**
Thermometer vs Minimum	51	0.999	1.29	−1.20	−2.14 to −0.26	0.953 (0.038 to 0.990)
Thermometer vs Maximum	51	0.999	0.35	0.20	−0.37 to 0.77	0.997 (0.988 to 0.999)
Thermometer vs Average	51	0.999	0.62	−0.50	−1.22 to 0.20	0.989 (0.754 to 0.997)
Thermometer vs Point	51	0.999	0.60	−0.36	−1.31 to 0.57	0.989 (0.955 to 0.996)

Note: Bias and LoA are expressed in °C as (IR – thermometer). ICC values are two-way random, absolute-agreement, single-measure ICCs with 95% confidence intervals.

Table 2. Proportional bias assessment using regression of paired differences (camera – thermometer) on the mean of the two methods.

Test 1 (2.9 L water, 20 cm; n = 87)				
Method	**n**	**Slope**	**95% CI**	**p-value**
Thermometer vs Minimum	87	0.068	0.041 to 0.095	<0.001
Thermometer vs Maximum	87	−0.145	−0.159 to −0.131	<0.001
Thermometer vs Average	87	−0.171	−0.186 to −0.155	<0.001
Thermometer vs Point	87	−0.154	−0.172 to −0.135	<0.001
Test 2 (1.5 L water, 30 cm; n = 51)				
Method	**n**	**Slope**	**95% CI**	**p-value**
Thermometer vs Minimum	51	−0.104	−0.119 to −0.089	<0.001
Thermometer vs Maximum	51	−0.043	−0.058 to −0.028	<0.001
Thermometer vs Average	51	−0.069	−0.084 to −0.055	<0.001
Thermometer vs Point	51	−0.098	−0.116 to −0.080	<0.001

Note: A non-zero slope indicates proportional bias (i.e. differences vary across the measurement range).

to −0.26 °C; RMSE 1.29 °C) and showed a wider ICC confidence interval (0.953, 95% CI 0.038–0.990) than the other outputs. Across both tests, Spearman correlation coefficients (ρ) were ≥ 0.995 for all comparisons (Table 1). A proportional-bias check indicated that differences were not fully constant across the measurement range (Table 2); therefore, Bland-Altman agreement metrics were interpreted within the tested range. Taken together, these results indicate that Avg and Pt provide the closest tracking of thermometer readings under both experimental

conditions, whereas Min should not be considered a reliable estimator of bulk water temperature.

Cadaver jejunal thermal contrast model

The results of the cadaver experiment are illustrated in Figures 5 and 6 and are based on the infrared images acquired with the InfiRay P2 Pro camera. At baseline, the exposed jejunal loop exhibited a homogeneous temperature distribution, as indicated by the uniform color pattern following the anatomical contours of the bowel in the thermal image.

After isolation of a jejunal segment and intraluminal injection of warm water, a clear temperature difference became visible (Figures 5C and 5D). The ligated segment appeared markedly warmer than the surrounding intestine, with a color gradient from cooler (darker) areas to warmer (brighter) tones. A Pt measurement on an adjacent, the non-manipulated segment (P2) showed a surface temperature of 24.4 °C, whereas the water-filled segment (P1) reached 30.4 °C, yielding a temperature difference (ΔT = P1 − P2) of approximately 6.0 °C. This thermal pattern corresponded closely with the anatomical boundaries created by the ligatures.

In the mesenteric venous warming model, injection of warm water into a mesenteric vein produced a linear track of increased temperature along the venous course and in the drained intestinal segment. Although this part of the experiment was primarily qualitative, the thermal images clearly demonstrated a contiguous warm pattern along the vein and into the bowel wall, whereas the adjacent intestines retained lower surface temperatures.

In the in situ intraluminal warming procedure, after reinserting a warm water–filled jejunal segment into the abdominal cavity, the infrared camera still readily identified the injected loop as a focal area of increased temperature against the background of surrounding bowel. Point measurements showed a temperature of 35.6 °C for the warmed segment (P1) versus 25.7 °C for the adjacent, non-manipulated segment (P2), resulting in a ΔT of about 9.9 °C, as shown in Figure 6D.

DISCUSSION

The InfiRay P2 Pro smartphone-attached infrared camera was successfully tested in two thermography models. The water-bath experiment showed close agreement between the smartphone-based infrared camera and the reference thermometer, particularly for the Avg and Pt outputs, whereas the Min output consistently underestimated the reference temperature. In the cadaver model, the camera visualized local surface temperature differences along the jejunum and detected pronounced, anatomically coherent thermal contrast. These cadaver findings provided evidence that the system can detect surface temperature demarcation, although further validation as tool to assess intestinal perfusion or tissue viability still needs to be performed.

In the water-bath experiments, the infrared camera closely tracked the reference thermometer across the full temperature range. However, for surgical applications, the magnitude and stability of disagreement are more important than correlation alone. Bland-Altman analysis indicated that the Avg and Pt outputs provided the most reliable readouts, with small deviations from the thermometer across both experimental setups. However, because measurements were obtained serially during cooling, these agreement estimates should be regarded as descriptive for the tested temperature range. These results are broadly consistent with proposed performance standards for medical infrared systems, where deviations of approximately 0.5–1.0 °C are considered acceptable and differences of 1.0–1.5 °C may already be relevant when relative temperature differences are interpreted (Lahiri et al., 2012; Kesztyüs et al., 2023).

The present results also clarify how different camera outputs should be interpreted. Because the contact thermometer samples at a single point within the water volume, Avg (mean ROI temperature) and Pt (a point adjacent to the probe tip) provide the most meaningful infrared comparators. In contrast, Min and Max values are derived from single pixels anywhere within the ROI and primarily reflect local surface phenomena, such as small air bubbles, ripples, glare artefacts, or local convection currents rather than the bulk temperature at the probe location. Accordingly, Min consistently underestimated the thermometer readings and showed wider limits of agreement, supporting recommendations to rely on mean ROI temperatures for quantitative reporting. Clinically, this means that a single unusually “cold” or “hot” pixel should not be interpreted as focal pathology unless it is spatially coherent and persists across repeated frames and measurements (Lahiri et al., 2012; Casas-Alvarado et al., 2022). Max showed only a small tendency to overestimate temperature and may help highlight local hotspots within the ROI, thereby complementing Avg and Pt when temperature distribution across the surface is heterogeneous.

On this technical foundation, the key question for the practicing surgeon is whether the observed measurement error would compromise intra-operative decision-making. Current assessment of intestinal viability relies on color, peristalsis and bleeding, yet is inherently subjective, with reported sensitivity as low as 38-62% and specificity of 46-52% (Mullen et al., 2020). In this context, IRT would not be expected to replace conventional judgement, but rather to provide a rapid adjunct that highlights conspicuous thermal demarcation between adjacent segments when gross assessment is equivocal.

Against that background, a thermographic tool that systematically underestimates absolute temperature by less than 1 °C yet consistently displays clear temperature differences of several degrees between adjacent loops, is unlikely to be limited by this degree of measurement error, and pending clinical validation could provide a more objective and reproducible visualization of relative surface temperature patterns than subjective inspection alone. This interpretation

is consistent with experimental work in porcine intestinal models, where infrared thermography is used in a semi-quantitative manner to visualize temperature boundaries between well-perfused and devascularized segments and to select resection margins based on relative temperature differences rather than a single absolute cut-off value (Bernard et al., 2019). Similarly, in human laparoscopic colorectal surgery, intra-operative thermography has been applied to compare the temperature of the residual and resected bowel at the planned transection line, with a temperature difference of approximately 2-3 °C between these segments correlating with fluoroscopic perfusion indices (Tokunaga et al., 2021). Together, these data support the concept that the primary clinical value of thermography lies in detecting relative temperature differences between adjacent intestinal segments, while moderate absolute measurement error may be acceptable if relative contrast is preserved.

The cadaver experiment was designed as a proof of concept rather than quantitative validation, but the observed thermal contrasts were large and anatomically coherent. In the ex vivo intraluminal warming procedure, the temperature difference between the warmed segment (P1) and adjacent non-manipulated intestine (P2) was approximately 6 °C, with the warmed loop clearly demarcated on the thermal image. In the in-situ scenario, after the warmed segment was replaced into the abdomen, ΔT between P1 and P2 approached 10 °C and the injected loop remained easily distinguishable from the surrounding bowel segments. Whereas the present model created a local temperature increase by design, experimental porcine intestinal resection work has shown that devascularized bowel can be differentiated from adjacent vascularized segments based on relative temperature contrasts (Bernard et al., 2019), supporting the concept that thermal demarcation may be useful as an adjunctive parameter in intestinal viability assessment. These differences markedly exceed the measurement error quantified in the water-bath model, suggesting that the observed contrasts reflect true thermal

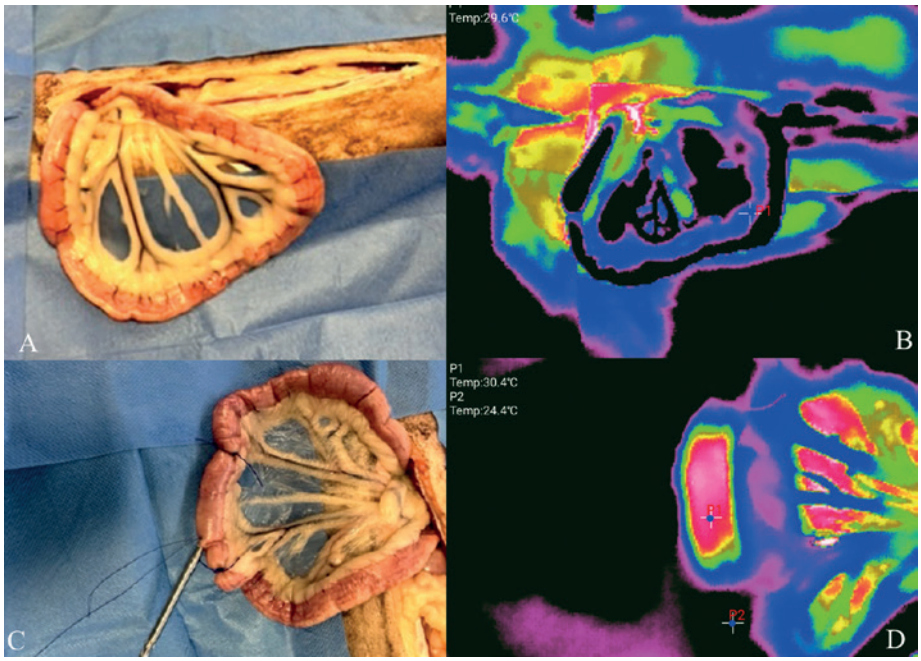

Figure 5. Jejunum before manipulation (A). Corresponding InfiRay P2 Pro image (B). Jejunum with ligatures and injected with warm water (46.10 °C) (C). Corresponding InfiRay P2 Pro image (D).

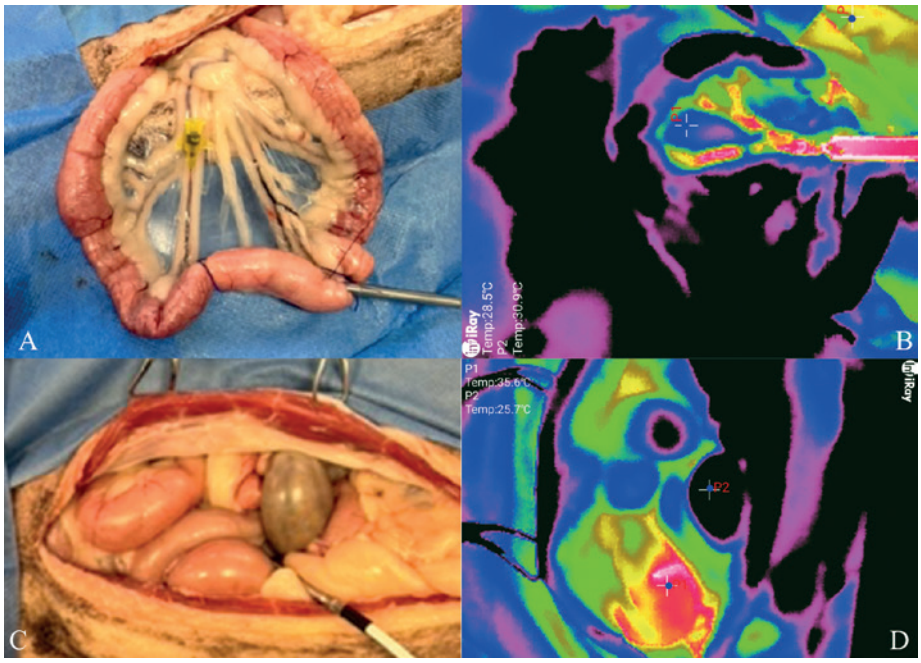

Figure 6. Jejunum with a catheter in a mesenterial vein (A). InfiRay P2 Pro image showing warm water (44.30 °C) injected in the mesenteric vein (B). In situ jejunum with a warm-water-injected jejunal segment (C). Corresponding InfiRay P2 Pro image (D).

signal rather than instrumental noise. In addition, mesenteric venous warming produced a continuous thermal track along the injected vein and into the drained bowel, illustrating that the camera can visualize linear surface temperature patterns associated with the warmed mesenteric vessel course.

These findings are in line with experimental intestinal studies in pigs, where thermography has been used to delineate perfused from non-perfused bowel and to support the choice of resection margins based on relative temperature patterns (Bernard et al., 2019). In dogs undergoing

laparotomy for small intestinal foreign body obstruction, intra-operative thermography using a handheld IRT radiometric thermal camera (FLIR E6 WiFi) did not detect significant spatial serosal temperature differences between the obstruction site and the adjacent oral/aboral segments. However, when comparing the obstruction site before versus immediately after surgical resolution, the serosal temperature measured directly over the obstruction decreased by a median of approximately 2.4 °C, indicating that IRT may capture dynamic local temperature changes during surgery rather than static between-segment contrasts (Finstad et al., 2023). This clinical situation is not directly comparable to porcine devascularization models, where the thermal contrast is driven by clear-cut differences between perfused and non-perfused bowel and is therefore usually more pronounced. Although Finstad et al. (2023) used a different IRT camera system, their findings still support the general principle that intra-operative thermography can capture local surface temperature dynamics, in line with the marked ΔT observed in the present cadaver model using a compact smartphone-based camera.

This research should be interpreted as preliminary. The cadaver study was performed in a single dog, temperature gradients were induced by warm-water injection rather than true ischemia reperfusion, and no histological or perfusion gold standard or ROC analysis was available to define diagnostic ΔT thresholds. In addition, the in-situ simulation created a segment that was warmer than its surroundings, which is the reverse of the expected contrast when a focal ischemic segment is embedded in normally perfused bowels. In live patients, passive heat transfer from adjacent healthy tissue, as well as differences in wall thickness, surface moisture and ambient conditions, may therefore modify the thermal patterns observed in this cadaver model and could make subtle perfusion defects more difficult to detect. Moreover, the cadaver data were analyzed descriptively. Therefore, in future research, smartphone-based IRT should be evaluated in live dogs with intestinal pathology using repeated measurements across multiple patients and standardized acquisition protocols, given the sensitivity of IRT to biological, environmental and technical sources of variability (Loughin and Marino, 2007; Fernández-Cuevas et al., 2015; Nomura et al., 2018; Casas-Alvarado et al., 2022; Whittaker et al., 2023). Specifically, intra-operative factors, such as camera distance and angle, exposure time, intra-abdominal fluid and inter-observer ROI placement should be quantified to define robust operating conditions before routine use can be recommended.

Overall, the cadaver experiments showed that the smartphone-based infrared camera could visualize pronounced, anatomically coherent differences in jejunal surface temperature under both isolated and in situ conditions. These findings support further evaluation of this low-cost system for visualizing intra-operative thermal contrast, but they do not establish diagnostic accuracy for intestinal perfusion or viability.

REFERENCES

Bagavathiappan S., Saravanan T., Philip J., Jayakumar T., Raj B., Karunanithi R., Panicker T.M.R., Korath M.P., Jagadeesan K. (2009). Infrared thermal imaging for detection of peripheral vascular disorders. *Journal of Medical Physics 34*, 43-47.

Bernard V., Staffa E., Pokorná J., Čan V., Farkašová M., Zetelová A., Kala Z. (2019). Semi-quantitative comparison of infrared thermography with indocyanine green imaging in porcine intestinal resection. *IRBM.* 2019 40, 307-312.

Casas-Alvarado A., Mota-Rojas D., Hernández-Ávalos I., Mora-Medina P., Olmos-Hernández A., Verduzco-Mendoza A., Lezama-García K., Martínez-Burnes J. (2020). Advances in infrared thermography: Surgical aspects, vascular changes, and pain monitoring in veterinary medicine. *Journal of Thermal Biology 92*, 102664.

Casas-Alvarado A., Martínez-Burnes J., Mora-Medina P., Hernández-Avalos I., Domínguez-Oliva A., Lezama-García K., Gómez-Prado J., Mota-Rojas D. (2022). Thermal and circulatory changes in diverse body regions in dogs and cats evaluated by infrared thermography. *Animals 12*, 789.

Ferlini Agne G., Adamson K., McGlinchey L., Kravchuk O., Santos L., Schumacher J. (2024). Comparison of a hand-held high-end resolution infrared thermography (FLIR P640) and a smartphone infrared thermographic device (FLIR One) for the assessment of skin surface temperature after anaesthetising the median nerve in healthy horses. *Plos one 19*, e0309603.

Fernández-Cuevas I., Bouzas Marins J.C., Arnáiz Lastras J., Gómez Carmona P.M., Piñonosa Cano S., García-Concepción M.Á., Sillero-Quintana M. (2015). Classification of factors influencing the use of infrared thermography in humans: A review. *Infrared Physics & Technology 71*, 28-55.

Finstad J.B., Cooper E., ten Cate S.C., Yaxley P., Her J., Guillaumin J. (2023). Infrared thermography is a novel tool to assess small intestinal surface temperature in dogs undergoing laparotomy for foreign body obstruction. *American Journal of Veterinary Research 84*, 1-9.

Fridberg M., Bafor A., Iobst C.A., Laugesen B., Jepsen J.F., Rahbek O., Kold S. (2024). The role of thermography in assessment of wounds: A scoping review. Injury *55*, 111833.

Giggin T., Jennes D., Sainulabdeen A., John Martin K.D. (2023). Infrared thermography as an adjunct tool for the diagnosis of fracture in a racing buffalo bull: A case report. Journal of Veterinary Physiology and Pathology *2*, 1-4. DOI: 10.58803/JVPP.2023.2.1.01.

Huynh M. (2019). Smartphone-based device in exotic pet medicine. *Veterinary Clinics of North America: Exotic Animal Practice 22*, 349-366.

Sung J., Loughin C.A., Marino D.J., Leyva F., Dewey C.W., Umbaugh S., Lesser M. (2019). Medical infrared thermal imaging of canine appendicular bone neoplasia. *BMC Veterinary Research 15*, 430.

Kesztyüs D., Brücher S., Wilson C., Kesztyüs T. (2023). Use of infrared thermography in medical diagnosis, screening, and disease monitoring: A scoping review. *Medicina* 59, 2139.

Lahiri B.B., Bagavathiappan S., Jayakumar T., Philip J. (2012). Medical applications of infrared thermography: A review. *Infrared Physics & Technology 55*, 221-235.

Loughin C.A., Marino D.J. (2007). Evaluation of thermographic imaging of the limbs of healthy dogs. *American Journal of Veterinary Research 68*, 1064-1069.

McManus C., Tanure C.B., Peripolli V., Seixas L., Fischer V., Gabbi A.M., Menegassi S.R.O., Stumpf M.T., Kolling G.J., Dias E., Costa J.B.G. (2016). Infrared thermography in animal production: An overview. *Computers and Electronics in Agriculture 123*, 10-16.

Mota-Rojas, D., Olmos-Hernández, A., Verduzco-Mendoza, A., Lecona-Butrón, H., Martínez-Burnes, J., Mora-Medina, P., Gómez-Prado, J., Orihuela, A.. (2021). Infrared thermal imaging associated with pain in laboratory animals. *Experimental Animals* 70, 1-12.

Mullen K.M., Regier P.J., Ellison G.W., Londoño L. (2020). The pathophysiology of small intestinal foreign body obstruction and intraoperative assessment of tissue viability in dogs: A review. *Topics in Companion Animal Medicine 40*, 100438.

© 2026 by the authors. Licensee Vlaams Diergeneeskundig Tijdschrift, Ghent University, Belgium. This article is an open access article distributed under the terms and conditions of the Creative Commons Attribution (CC BY) license (http://creativecommons.org/licenses/by/4.0/).